PNAS RESEARCH ARTICLE | IMMUNOLOGY AND INFLAMMATION

Divergent roles for STAT4 in shaping differentiation of cytotoxic ILC1 and NK cells during gut inflammation

Gianluca Scarno[a,b,1,2], Julija Mazej[a,b,1], Mattia Laffranchi[a,b], Chiara Di Censo[a,b], Irene Mattiola[c,d], Arianna M. Candelotti[a,b], Giuseppe Pietropaolo[a,b], Helena Stabile[a,b], Cinzia Fionda[a,b], Giovanna Peruzzi[e], Stephen R. Brooks[f], Wanxia Li Tsai[g], Yohei Mikami[h], Giovanni Bernardini[a,b], Angela Gismondi[a,b], Silvano Sozzani[a,b,i], James P. Di Santo[j], Christian A. J. Vosshenrich[j], Andreas Diefenbach[c,d], Massimo Gadina[g], Angela Santoni[a,b,i], and Giuseppe Sciumè[a,b,2]

Edited by Marco Colonna, Washington University in St. Louis School of Medicine, St. Louis, MO; received May 4, 2023; accepted August 10, 2023

Natural killer (NK) cells and type 1 innate lymphoid cells (ILC1) require signal transducer and activator of transcription 4 (STAT4) to elicit rapid effector responses and protect against pathogens. By combining genetic and transcriptomic approaches, we uncovered divergent roles for STAT4 in regulating effector differentiation of these functionally related cell types. *Stat4* deletion in *Ncr1*-expressing cells led to impaired NK cell terminal differentiation as well as to an unexpected increased generation of cytotoxic ILC1 during intestinal inflammation. Mechanistically, *Stat4*-deficient ILC1 exhibited upregulation of gene modules regulated by STAT5 in vivo and an aberrant effector differentiation upon in vitro stimulation with IL-2, used as a prototypical STAT5 activator. Moreover, STAT4 expression in NCR$^+$ innate lymphocytes restrained gut inflammation in the dextran sulfate sodium-induced colitis model limiting pathogenic production of IL-13 from adaptive CD4$^+$ T cells in the large intestine. Collectively, our data shed light on shared and distinctive mechanisms of STAT4-regulated transcriptional control in NK cells and ILC1 required for intestinal inflammatory responses.

innate lymphocytes | NK cells | JAK/STAT | transcriptional regulations | inflammation

Significance

Among innate lymphocytes, natural killer (NK) cells represent the prototypical cytotoxic cells. However, the spectrum of killer cells has recently expanded with the identification of innate lymphoid cells (ILCs) having cytotoxic functions. Our work reveals that deficiency of the transcription factor *Stat4* in mice leads to impaired NK cell differentiation and to a paradoxical increase of cytotoxic ILC1 during intestinal inflammation. These divergent effects rely on the ability of STAT4 to antagonize the function of cytokines activating STAT5 in ILC1. Targeting STAT4 in innate lymphocytes also leads to increased IL-13 production from T cells, which enhances colitis. Our findings shed light on distinct inflammatory circuits regulated by innate lymphocytes that can provide opportunities for therapeutic intervention in inflammatory bowel disease.

Innate lymphocytes patrol environmentally exposed interfaces by providing fast effector responses that are required to sustain barrier integrity and to defend against infection (1, 2). Among innate lymphocytes, natural killer (NK) cells represent the prototypical cytotoxic subset, while innate lymphoid cells (ILCs) are divided into three main "helper" groups, ILC1-3, based on their ability to produce polarized cytokine responses (3). ILC1 and NK cells elicit a potent type 1 response upon activation, characterized by production of the cytokine interferon (IFN)-γ, and the chemokines CCL3-5 and XCL1, as well as these cells are required for protection against intracellular pathogens (4, 5). Although NK cells and ILC1 have been considered as two functionally distinct cell types, the recent identification of cytotoxic ILC1 expressing perforin and granzymes as well as the recognition of plasticity enabling NK cells to acquire ILC1-like features have blurred the boundaries between these two populations (6–11).

The poised effector features of NK cells and ILC1 are established through a stepwise acquisition of DNA-accessible regulatory elements occurring during development and prior to the encounter of a pathogen (12, 13). Effector differentiation starts with the sequential downregulation of markers expressed by NK/ILC progenitors and immature cells and proceeds with the induction of genes encoding for effector molecules, including granzymes in ILC1, or adhesion molecules, such as CD11b and KLRG1 in NK cells (7, 14). At the transcriptional level, these functions are regulated by specific transcription factor (TF) networks, coordinated by the expression of the lineage-defining TFs T-bet and Eomes and by the signal-regulated TF STAT4 (15–17). Eomes is required for the development of NK cells, while T-bet sustains both terminal differentiation of NK cells and development of ILC1 (18–24). In contrast, the absence of STAT4 in mice is not associated with developmental defects or changes in the homeostatic numbers of both NK cells and ILC1 (25–28). Instead, when triggered by interleukin (IL)-12 or IFN-α/β, STAT4 plays fundamental roles in the initiation of effector responses by promoting fast release of type 1 cytokines in ILC1 and NK cells as well as by sustaining generation and proliferation of memory or adaptive-like NK cells (29–32). Both high-magnitude gene induction during acute activation and generation of adaptive-like NK cells require STAT4-dependent epigenetic regulation for the establishment of specific sets of accessible enhancers (33, 34).

Due to their capacity to promote potent inflammatory responses, prolonged activation of innate lymphocytes can lead to tissue damage and exacerbation of several inflammatory conditions, such as allergy, asthma, or inflammatory bowel disease (IBD) (1, 35, 36). ILCs

Author contributions: G. Scarno, A.G., S.S., J.P.D.S., C.A.J.V., A.D., M.G., A.S., and G. Sciumè designed research; G. Scarno, J.M., C.D.C., I.M., A.M.C., G. Pietropaolo, H.S., C.F., G. Peruzzi, W.L.T., Y.M., and G.B. performed research; G. Scarno, J.M., M.L., I.M., A.M.C., G. Pietropaolo, H.S., C.F., G. Peruzzi, S.R.B., Y.M., G.B., and G. Sciumè analyzed data; and G. Scarno and G. Sciumè wrote the paper.

The authors declare no competing interest.

This article is a PNAS Direct Submission.

[1]G.S. and J.M. contributed equally to this work.

[2]To whom correspondence may be addressed. Email: gianluca.scarno@uniroma1.it or giuseppe.sciume@uniroma1.it.

This article contains supporting information online at https://www.pnas.org/lookup/suppl/doi:10.1073/pnas.2306761120/-/DCSupplemental.

Published September 27, 2023.

are particularly enriched in the gut mucosal tissue playing either a protective role, by regulating intestinal homeostasis and tissue repair, or exerting pathogenic functions, by sustaining inflammation (37–39). The active colitis occurring in patients with IBD, including Crohn's disease (CD) and ulcerative colitis, is characterized by dysregulated expression of cytokines and alterations of ILC profiles both at the sites of inflammation and in the peripheral blood (40–42). In particular, type 1 innate lymphocytes accumulate in the inflamed intestinal epithelium of CD patients (41, 43), implying a role for IFN-γ-producing ILCs in the context of gut mucosal inflammation. Plasticity of ILC3 toward the type 1 fate has been proposed in humans as a main mechanism for this accumulation (44, 45). These transitions have been investigated in mice by using a *Rorc*-fate map (FM) reporter system, showing that ILC3-ILC1 plasticity can occur both at steady state and in pathological conditions (27, 46). While ILC3 are considered drivers of intestinal inflammation downstream of IL-23 (47), ablation of NK cells, using genetic approaches or administration of depleting antibodies, worsens intestinal inflammation in the mouse model of colitis induced by dextran sulfate sodium (DSS) administration (48, 49).

Being key mediators for signaling events downstream of many cytokine receptors, members of the STAT family are particularly relevant in the pathogenesis of IBD (42, 50). This is supported by a strong association between genetic variants in the Janus kinase (JAK)/STAT pathway and risk of developing this pathology as well as by the recent success of JAK inhibitors for the treatment of IBD (51–53). While the functions of STAT4 have been extensively investigated in several contexts of the NK cell response to pathogens, whether this TF can control effector phenotypes of innate lymphocytes or can impact intestinal inflammation still remains poorly investigated.

Herein, by generating a mouse model allowing conditional deletion of the *Stat4* gene in innate lymphocytes, we showed that this TF has critical functions during acute intestinal inflammation. *Stat4* deletion in NCR$^+$ innate lymphocytes led to systemic and local effects during DSS-induced colitis, including dysregulation of the serum levels of IFN-γ as well as increased pathogenic production of IL-13 from CD4$^+$ T lymphocytes, in the large intestine. Single-cell RNA-seq analysis revealed divergent roles for STAT4 in controlling effector differentiation of ILC1 and NK cells during intestinal inflammation. While STAT4 was required for inflammation-induced NK cell terminal differentiation, its deletion in NCR$^+$ cells induced both a paradoxical increased generation of cytotoxic ILC1 and an altered ability of these cells to perceive cytokines using STAT5 for signaling. Utilizing an in vitro model, we established that *Stat4*-deficient ILC1 from distinct tissues exhibited an accelerated effector differentiation when cultured with IL-2, characterized by increased expression of granzymes.

Results

STAT4 Signaling in NCR$^+$ Innate Lymphocytes Restrains DSS-Induced Intestinal Inflammation. To measure STAT4 expression in large intestine lamina propria (lilp) innate lymphocytes, we employed intracellular flow cytometry using lilp cells isolated from wild-type (*Stat4*$^{+/+}$) mice (gating strategy in *SI Appendix*, Fig. S1*A*). NCR$^+$ innate lymphocytes (NKp46$^+$ cells), namely NK cells, ILC1, and NCR$^+$ ILC3, expressed high levels of STAT4, whereas no signal was detected in ILC2 and NCR$^-$ ILC3 (*SI Appendix*, Fig. S1*B*). In agreement with these results, short stimulation with IL-12 triggered phosphorylation of STAT4 (pSTAT4) in NK cells and ILC1, as well as in a fraction of NCR$^+$ ILC3 (*SI Appendix*, Fig. S1*C*). Given the selective expression of STAT4 in lilp NCR$^+$ innate lymphocytes, we generated a mouse model allowing for conditional deletion of the *Stat4* exon 3 specifically in NKp46$^+$ cells, by breeding *Stat4*$^{fl/fl}$ mice (generated in this study) with *Ncr1*^{greenCre} mice (54), named here as *Ncr1*$^{\Delta Stat4}$ mice (*SI Appendix*, Fig. S1*D*). The analysis of total- and phospho-STAT4 levels confirmed that both forms of the protein were efficiently ablated in NCR$^+$ innate lymphocytes isolated from *Ncr1*$^{\Delta Stat4}$ mice (*SI Appendix*, Fig. S1 *E* and *F*). Similar results were obtained using splenic NCR$^+$ cells (*SI Appendix*, Fig. S1*G*). The absence of STAT4 in *Ncr1*$^{\Delta Stat4}$ mice did not alter the homeostatic pool of large intestinal NCR$^+$ cells (*SI Appendix*, Fig. S1 *H* and *I*), consistent with previous findings obtained by using mice carrying germline deletion of *Stat4* (27, 28, 55). Similarly, *Ncr1*$^{\Delta Stat4}$ mice did not show either intrinsic defects in the pool of total NCR$^+$ innate lymphocytes in other tissues, such as the spleen, liver, and bone marrow (*SI Appendix*, Fig. S1*J*) or extrinsic effects on other lilp immune cell types, including T helper (Th) cells and regulatory T cells (Tregs) (*SI Appendix*, Fig. S1*K*). In addition, we found no recruitment of neutrophils in both mouse groups (*SI Appendix*, Fig. S1*L*), indicating that STAT4 expression in innate lymphocytes is not critical at steady state.

To induce pathological perturbation in the large intestine, we administered DSS to mice in the drinking water for 7 d. First, we profiled the features of innate lymphocytes during colitis by using *Stat4*$^{+/+}$ mice. DSS-induced inflammation was characterized by a significant increase of NK cells in the lilp of treated mice, compared with mice left untreated, while the number of other ILC subsets remained unaltered (*SI Appendix*, Fig. S2 *A* and *B*). Within the first 3 d of DSS treatment, lilp ILC1 were more abundant than NK cells and represented the main source of IFN-γ, as evaluated after ex vivo stimulation with IL-12 (*SI Appendix*, Fig. S2 *C* and *D*). NK cells, instead, increased over time, overcoming ILC1 both in terms of frequency and potential to produce IFN-γ, as observed at days 5 and 7 of DSS treatment (*SI Appendix*, Fig. S2 *D* and *E*). The increased expression levels of IFN-γ and the global activation state of NK cells during colitis were confirmed by performing bulk RNA-seq of lilp NK cells from *Stat4*$^{+/+}$ mice treated with DSS for 7 d, compared with splenic NK cells isolated from mice left untreated, as control. Differential expression analysis revealed a total of 244 induced genes in lilp NK cells, including transcripts conventionally associated with NK cell activation, such as *Ifng*, *Gzmb*, *Ccl3*, *Ccl4*, *Cd69,* and *Cish* (*SI Appendix*, Fig. S2*F* and Dataset S1 for full gene list).

To evaluate the role of STAT4 expression in innate lymphocytes during intestinal inflammation, we next challenged both *Stat4*$^{fl/fl}$ and *Ncr1*$^{\Delta Stat4}$ mice with DSS for 7 d. Flow cytometry analysis revealed no major differences in the frequency of NCR$^+$ innate lymphocytes (Fig. 1*A* and *SI Appendix*, Fig. S2*G*), indicating that STAT4 was neither required for the accumulation of lilp NK cells nor necessary to control the numbers of ILC1 or NCR$^+$ ILC3 during intestinal inflammation. In contrast, FACS-sorted lilp NK cells and ILC1 isolated from *Ncr1*$^{\Delta Stat4}$ mice treated for 7 d with DSS failed to produce IFN-γ either when left untreated or stimulated with IL-12 (Fig. 1*B*). This defect led to an overall decrease of the serum levels of IFN-γ in DSS-treated *Ncr1*$^{\Delta Stat4}$ mice (Fig. 1*C*), underlining the importance of STAT4 expression in innate lymphocytes in the establishment of the systemic IFN-γ levels, during acute intestinal inflammation. Despite the critical role of STAT4 in promoting IFN-γ production in innate lymphocytes, *Ncr1*$^{\Delta Stat4}$ mice were more susceptible to develop intestinal inflammation, showing higher body weight loss and Disease Activity Index (DAI) than littermate *Stat4*$^{fl/fl}$ mice (Fig. 1 *D* and *E* and *SI Appendix*, Fig. S2*H*).

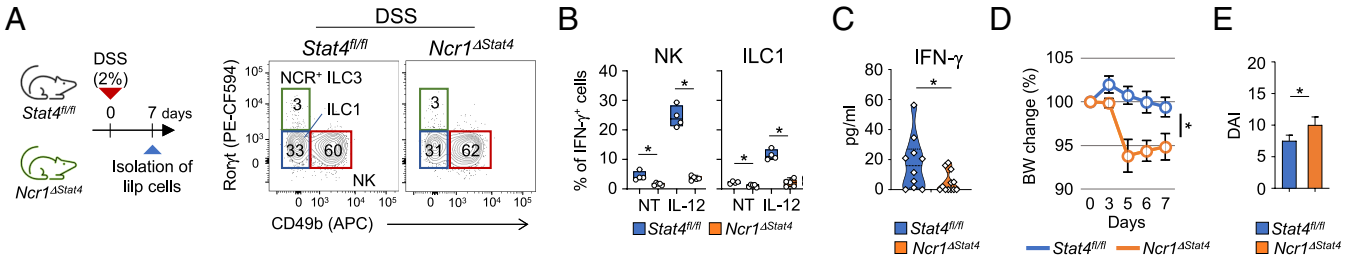

Fig. 1. STAT4 expression in NCR$^+$ innate lymphocytes limits intestinal inflammation. (*A*) Full gating strategy for prototypical NK/ILC subsets in the lilp in *SI Appendix*, Fig. S1*A*. Cells were isolated from the lilp of DSS-treated (day 7) *Stat4*$^{fl/fl}$ and *Ncr1*$^{\Delta Stat4}$ mice. Flow cytometry contour plot of NCR$^+$ innate lymphocytes showing the frequency of NK cells, ILC1, and NCR$^+$ ILC3 in the lilp of DSS-treated *Stat4*$^{fl/fl}$ and *Ncr1*$^{\Delta Stat4}$ mice. Representative flow panel of at least three independent experiments performed; n = 3 to 5 per group for each experiment. (*B*) Box plots show the percentage of IFN-γ$^+$ NK cells and ILC1 from the lilp of DSS-treated *Stat4*$^{fl/fl}$ and *Ncr1*$^{\Delta Stat4}$ mice, left untreated (NT) or upon ex vivo restimulation with IL-12 (100 ng/mL) for 8 h. Data from two independent experiments performed are shown; each plot represents an individual mouse. (*C*) The violin plot shows the concentration of IFN-γ, measured by ELISA, in the serum collected from DSS-treated *Stat4*$^{fl/fl}$ (n = 10) and *Ncr1*$^{\Delta Stat4}$ (n = 12) mice. (*D*) The line chart depicts the body weight change, expressed as a percentage of initial weight, in DSS-treated *Stat4*$^{fl/fl}$ (n = 18) and *Ncr1*$^{\Delta Stat4}$ mice (n = 21). Data provided represent the mean ± SEM of the percentage body weight of pooled data from four independent experiments. (*E*) The bar plot shows the DAI for *Stat4*$^{fl/fl}$ (n = 7) and *Ncr1*$^{\Delta Stat4}$ (n = 7) mice of pooled data from two independent experiments. For statistical analysis, unpaired Student's *t* test (*B*, *C*, and *E*) and Wilcoxon signed-rank test (*D*) were used.

These data provide evidence for a protective role of STAT4 expression in NCR$^+$ innate lymphocytes during DSS-induced intestinal inflammation.

STAT4 Limits Effector Differentiation of ILC1 during Acute Colitis. To further evaluate the impact of *Stat4* deletion on the phenotype and function of NCR$^+$ innate lymphocytes, we FACS-sorted NKp46$^+$ cells from DSS-treated *Stat4*$^{fl/fl}$ and *Ncr1*$^{\Delta Stat4}$ mice and assessed their transcriptomes by single cell RNA-sequencing (scRNA-seq) (Fig. 2*A*). The analysis of the transcriptional states of NCR$^+$ innate lymphocytes led to the identification of 10 distinct clusters, which we assigned to NK cells (clusters: a-e), ILC1 (a-d), and ILC3 (one cluster), based on the expression of the lineage-defining TF-encoding genes *Eomes*, *Tbx21,* and *Rorc* as well as of markers used by convention to discriminate NK cells and ILC1, such as *Cd200r1*, *Itga1* (encoding for CD49a), *Itga2* (CD49b), and *Il7r* (CD127; Fig. 2*A*, *SI Appendix*, Fig. S3*A*, and Dataset S2 for the full list of genes defining the distinct clusters). To obtain a global view of the genes regulated by STAT4 in total NK cell, ILC1 and NCR$^+$ ILC3 populations, we first performed pseudo-bulk differential expression analysis. Deletion of *Stat4* led to a higher number of differentially expressed genes (DEGs) in ILC1 compared with NK cells (37 and 21 genes, respectively, Fig. 2*B* and Dataset S3); no DEGs were found instead in NCR$^+$ ILC3. As compared to NK cells, *Stat4*-deficient ILC1 showed a higher proportion of up-regulated genes (10 vs. 3, Fig. 2*B*). Among DEGs, genes specifically down-regulated in ILC1 or NK cells comprised *Furin*, *Cxcr6*, *Icam1,* and *Stat3*; while *Pim2*, *Mxd1*, and *Enpp4* were significantly down-regulated both in ILC1 and NK cells (Fig. 2*C*). We also found that *Ccl5* transcript was significantly up-regulated in ILC1, while decreased in NK cells (Fig. 2*C*), indicating that opposite mechanisms of regulation are in place for this gene in the two subsets. Differential STAT4-dependent regulation of gene expression in NK cells and ILC1 was validated at the protein level for ICAM and CXCR6 by flow cytometry (Fig. 2*D*). Since no genes were significantly altered in NCR$^+$ ILC3 and because these cells are redundant in several models of intestinal inflammation/infection in T cell-competent mice (56, 57), we next focused on ILC1 and NK cells.

We next sought to define whether the transcriptional changes observed in NK cells and ILC1 also reflected alterations in the frequencies of the distinct clusters. By performing differential abundance analysis, we found no major differences in the frequency of the five NK cell states and the NCR$^+$ ILC3 cluster associated with *Stat4* deletion, while we observed a significant accumulation of the ILC1$_d$ cluster in *Ncr1*$^{\Delta Stat4}$ mice (Fig. 2*E*), suggesting a role for STAT4 in limiting this transcriptional state. To establish the phenotype of the ILC1 population that specifically expanded in *Ncr1*$^{\Delta Stat4}$ mice, we next evaluated the genes defining the different clusters. In both *Stat4*$^{fl/fl}$ and *Ncr1*$^{\Delta Stat4}$ mice, the four ILC1 transcriptional states delineated a continuum of cells characterized by the expression of genes, including *Icos, Rora*, *Serpinb1a*, and *Odc1* that were higher in ILC1$_{a\text{-}b}$; *Jun*, *Rgs1*, and *Klf6*, which identified ILC1$_c$, and *Itga1, Gzmc,* and *Il21r* defining the cluster of ILC1$_d$ (Fig. 2*F*). This expression profile was in agreement with the current model of liver ILC1 effector differentiation, which is characterized by a transition of ILC1 with helper functions to cells expressing granzymes and acquiring cytotoxic abilities (7, 58). Differential expression analysis obtained by comparing the distinct ILC1 transcriptional states from *Stat4*$^{fl/fl}$ and *Ncr1*$^{\Delta Stat4}$ mice revealed that cells belonging to the ILC1$_d$ cluster were the most affected by *Stat4* deletion (10 DEGs), followed by ILC1$_b$ (9 DEGs), and ILC1$_{a,c}$ (1 DEG for each cluster, gene list in Dataset S3). To determine whether the enrichment of the ILC1$_d$ cluster in *Ncr1*$^{\Delta Stat4}$ mice matched an increased effector differentiation, we tracked the ILC1 phenotype by flow cytometry, using expression of Inducible T Cell Costimulator (ICOS) and GzmC as markers for early and terminal differentiation, respectively. Lilp ILC1 from DSS-treated *Stat4*$^{fl/fl}$ mice showed a significant increase of ICOS$^+$ cells and minor changes in the expression of GzmC compared to mice left untreated (Fig. 2*G*). In contrast, we found that the intestinal inflammation skewed *Stat4*-deficient lilp ILC1 toward an ICOS$^-$GzmC$^+$ phenotype (Fig. 2*G*).

Altogether, these data provide evidence for a role of STAT4 in limiting ILC1 effector differentiation during intestinal inflammation.

Differential Contribution of ILC3- and NK Cell- Plasticity toward the GzmC$^+$ ILC1 Phenotype during Intestinal Inflammation. To evaluate the effector differentiation of lilp ILC1, we next performed trajectory analysis, which delineated a decreased expression of *Rora*, *Il7r*, and *Icos* and a parallel increased expression of *Gzmc* (*SI Appendix*, Fig. S3*B*). We validated the gradient expression of ICOS, CD127, and CD49a in lilp GzmC$^-$ and GzmC$^+$ ILC1 isolated from *Stat4*$^{+/+}$ mice treated or not with DSS by flow cytometry (*SI Appendix*, Fig. S3 *C* and *D*). Differing from hepatic cells, lilp ILC1 did not acquire high levels of GzmB and GzmA (*SI Appendix*, Fig. S3*E*) and did not extinguish the

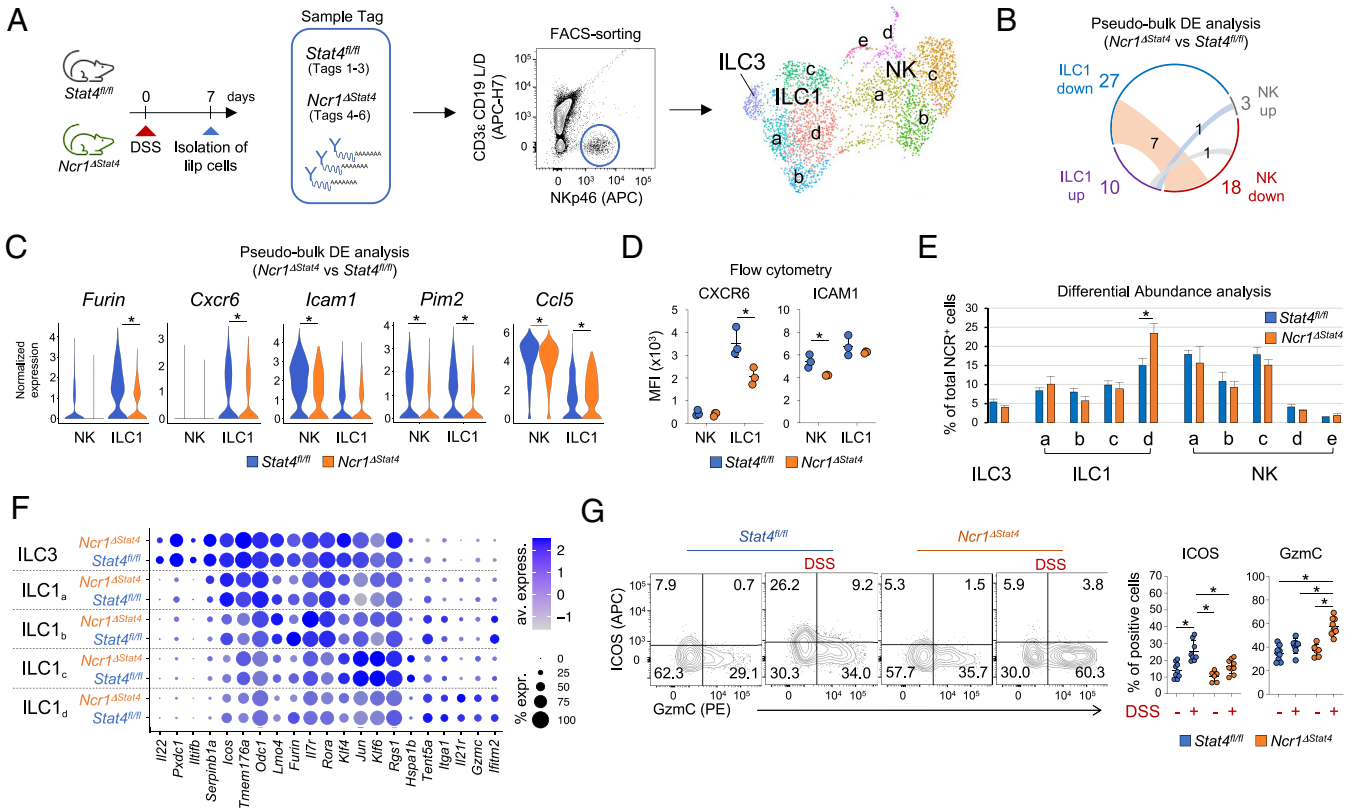

Fig. 2. Effects of *Stat4* deletion on the transcriptional states of NCR$^+$ innate lymphocytes in the inflamed lilp. (*A*) Schematic representation of single-cell RNA-seq workflow. Cells were isolated from the lilp of three *Stat4*$^{fl/fl}$ and three *Ncr1*$^{\Delta Stat4}$ mice after DSS treatment. NKp46$^+$ cells were sorted after sample tagging and processed for sequencing. UMAP shows the transcriptional states of lilp NK cells, ILC1, and ILC3 identified by scRNA-seq. (*B*) Circos visualization depicts the number of DEGs evaluated by pseudo-bulk analysis of lilp ILC1 and NK cells from *Stat4*$^{fl/fl}$ and *Ncr1*$^{\Delta Stat4}$ mice, treated with DSS for 7 d. A total of 27 genes were down-regulated in *Stat4*-deficient ILC1 (ILC1 down), while 10 genes were up-regulated (ILC1 up). Eighteen genes were down-regulated in *Stat4*-deficient NK cells (NK down), while 3 genes were up-regulated (NK up). Each connecting ribbon links the same genes across groups: Seven genes were down-regulated both in NK cells and ILC1 (salmon), 1 gene was up-regulated in both populations (light blue), and 1 gene was down-regulated in NK cells and up-regulated in ILC1 (light gray). (*C*) Violin plots depict the expression of *Furin*, *Cxcr6*, *Pim2*, *Icam1*, and *Ccl5* transcripts in lilp ILC1 and NK cells from *Stat4*$^{fl/fl}$ and *Ncr1*$^{\Delta Stat4}$ mice treated with DSS for 7 d. (*D*) Scatter plots show the expression of CXCR6 and ICAM1 in NK cells and ILC1 from the lilp of DSS-treated *Stat4*$^{fl/fl}$ and *Ncr1*$^{\Delta Stat4}$ mice treated with DSS for 7 d, evaluated by flow cytometry. A representative experiment out of two performed is shown; n = 3 per group. (*E*) The histogram plot depicts the frequency of cells belonging to the NK and ILC1/3 states in *Stat4*$^{fl/fl}$ and *Ncr1*$^{\Delta Stat4}$ mice treated with DSS for 7 d. Data are represented as mean ± SEM (n = 3 per group). (*F*) Top marker genes dividing NCR$^+$ innate lymphocytes into clusters were defined using the Seurat pipeline. The bubble plot displays the gene expression of top marker genes for ILC1, discriminated by genotype. (*G*) Flow cytometry contour plots show the expression of ICOS and GzmC in ILC1 isolated from the lilp of untreated control and DSS-treated *Stat4*$^{fl/fl}$ and *Ncr1*$^{\Delta Stat4fl/fl}$ mice. Scatter plots show the frequency of ICOS$^+$ (*Left*) and GzmC$^+$ (*Right*) ILC1 in the lilp of untreated control and DSS-treated *Stat4*$^{fl/fl}$ (blue) and *Ncr1*$^{\Delta Stat4}$ (orange) mice. (*G*) Data from three independent experiments performed are shown; n = 6 to 9 per group. For statistical analysis, unpaired Student's *t* test (*D*), two-way ANOVA (*E*), or one-way ANOVA (*G*) was used. *B* and *C* described in *SI Appendix*.

expression of CD127 and IL-18R1 (*SI Appendix*, Fig. S3 *D* and *F*), providing evidence for tissue-specific mechanisms of ILC1 effector differentiation. Trajectory analysis also highlighted a high similarity between less differentiated ILC1 and NCR$^+$ ILC3, raising the question as to what extent ILC3-ILC1 transition might give rise to ILC1 (namely exILC3) expressing granzymes in the large intestine. By employing Rorc(γt)-FM reporter mice, we revealed that Rorγt-FM$^+$ cells represented between 20 and 30% of the total ILC1 fraction at steady state, while this frequency further increased during colitis reaching up to 40% of the total ILC1 (*SI Appendix*, Fig. S3*G*). However, Rorγt-FM$^+$ ILC1 expressed both ICOS and GzmC, similarly to Rorγt-FM$^-$ cells (*SI Appendix*, Fig. S3*H*), indicating that after conversion, exILC3 underwent shared mechanisms of effector differentiation with ILC1. Next, to rule out a possible contribution of NK-ILC1 plasticity in establishing the pool of ILC1 in colitis settings, CD45.2$^+$ NK cells were adoptively transferred into mice carrying the CD45.1 allele, which were then treated with DSS for 7 d or left untreated. While inflammation was necessary for accumulation of NK cells in the large intestine, transferred cells maintained a CD49b$^+$ phenotype 7 d after DSS treatment (*SI Appendix*, Fig. S3*I*), indicating that NK cell identity was stable in these settings.

Thus, by using fate mapping and adoptive transfer approaches, we established lineage relationships of lilp NCR$^+$ innate lymphocytes during acute intestinal inflammation.

STAT4 Supports Inflammation-Driven Terminal Differentiation of NK Cells. Given the effect of *Stat4* deletion on ILC1 effector phenotype, we next sought to establish whether this TF could control aspects of NK cell differentiation that were not revealed by using pseudo-bulk analysis of total NK cells. Thus, we first defined the features of the five NK cell clusters in *Stat4*$^{fl/fl}$ and *Ncr1*$^{\Delta Stat4}$ mice that we identified by scRNA-seq (Fig. 2*A*). Cells assigned to the NK$_{d\text{-}e}$ clusters were enriched for genes encoding for structural proteins and replicative complexes and represented only a minor fraction of NK cells; for this reason, these states were excluded from further analysis. Cells belonging to the NK$_a$ cluster were characterized by the expression of *Itgax* (encoding for CD11c), *Egr1*, and *Zfp36*, an RNA-binding protein recently associated with immature NK cells (59) and with regulation of cytokine production in ILC2 (60); NK$_b$ and NK$_c$, instead, were defined by high expression of granzymes, *Gzma-b*, and the chemokines *Ccl3-4* (Fig. 3*A*). NK$_{a\text{-}c}$ states also expressed distinct levels of *Cd27*, *Itgam* (encoding for CD11b), and *Klrg1* (*SI Appendix*, Fig. S4*A*), which

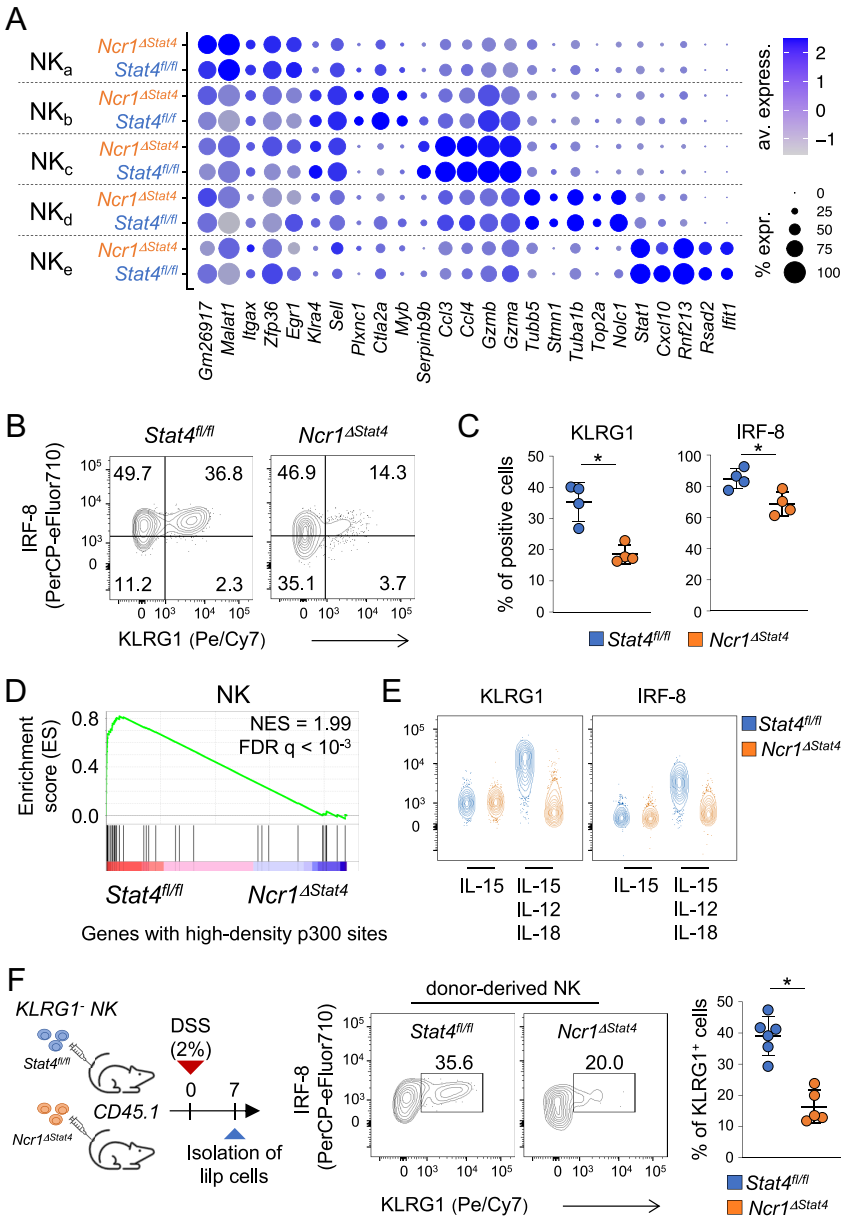

Fig. 3. STAT4 is required for terminal differentiation of NK cells. (*A*) Top marker genes dividing NCR$^+$ innate lymphocytes into clusters were defined using the Seurat pipeline. The bubble plot displays the gene expression of top marker genes for NK cells, discriminated by genotype. (*B*) The flow cytometry contour plot shows expression of KLRG1 and IRF-8 in lilp NK cells from DSS-treated *Stat4*$^{fl/fl}$ and *Ncr1*$^{\Delta Stat4}$ mice. (*C*) Scatter plot showing the percentage of KLRG1$^+$ and IRF-8$^+$ NK cells in the lilp of DSS-treated *Stat4*$^{fl/fl}$ and *Ncr1*$^{\Delta Stat4}$ mice. (*B* and *C*) Representative data from two independent experiments performed are shown; n = 4 per group per experiment. For statistical analysis, unpaired Student's *t* test was used. (*D*) GSEA plots for genes associated with high-density p300 load (established in ref. 33) in NK cells from *Stat4*$^{fl/fl}$ and *Ncr1*$^{\Delta Stat4}$ mice. (*E*) Flow cytometry contour plots showing the expression of KLRG1 (*Left*) and IRF-8 (*Right*) in FACS-sorted KLRG1$^-$ NK cells upon a 4 d-culture with IL-15 alone or IL-15, IL-12, and IL-18 (all at 10 ng/mL). Representative flow panels of two independent experiments performed are shown; n = 3 per group. (*F*) FACS-sorted KLRG1$^-$ NK cells from *Stat4*$^{fl/fl}$ and *Ncr1*$^{\Delta Stat4}$ mice were transferred into syngeneic CD45.1 mice. The flow cytometry contour plot shows the frequency of KLRG1 in donor-derived NK cells, isolated from the lilp of DSS-treated CD45.1 mice. The scatter plot shows the percentage of donor-derived KLRG1$^+$ NK cells in the lilp of DSS-treated mice. Data from two independent experiments performed are shown; n = 6 per group. For statistical analysis, unpaired Student's *t* test was used.

therefore represented the three main differentiation stages of NK cells (59). Differential expression analysis of the NK cell clusters showed that the NK$_c$ cluster was more affected by *Stat4* deletion (8 DEGs) than NK$_b$ (5 DEGs) and NK$_a$ (4 DEGs) clusters (gene list in Dataset S3). Although not detected by using a pseudo-bulk approach, *Stat4*-deficient NK$_c$ showed a reduced frequency of *Klrg1*-expressing cells, suggesting a defect in terminal differentiation (*SI Appendix*, Fig. S4*A*). By evaluation of the expression of genes defining mature NK cells (established in ref. 59), we found that *Stat4*-deficient NK cell clusters reached suboptimal expression of distinct genes, including *Klrg1*, *Itgam*, *Gzmb*, and *Irf8* (*SI Appendix*, Fig. S4*B*), further suggesting that *Stat4*-deficient NK cells could have impaired terminal differentiation during inflammation. In agreement with this hypothesis, *Ncr1*$^{\Delta Stat4}$ mice harbored less IRF-8^{high}KLRG1$^+$ NK cells than control mice upon DSS treatment (Fig. 3 *B* and *C* and *SI Appendix*, Fig. S4*C*). Reanalysis of available ChIP-seq data generated by using cytokine-activated NK cells (33) showed induction of STAT4 binding on the regulatory elements associated with the *Irf8* and *Klrg1* loci as well as a STAT4-dependent remodeling of the enhancer states nearby these two loci, as measured by analysis of p300 recruitment (*SI Appendix*, Fig. S4*D*). These data suggested that genes which require intensive enhancer remodeling

for expression might be highly affected by *Stat4* deletion during NK cell effector differentiation. To corroborate this hypothesis, we performed Gene Set Enrichment Analysis (GSEA), showing that genes associated with high-density p300 load (established in ref. 33) were mainly enriched in NK cells from *Stat4*$^{fl/fl}$ mice compared with *Ncr1*$^{\Delta Stat4}$ mice (Fig. 3*D*). We further validated the role of STAT4 in regulating effector differentiation of NK cells by using an in vitro model based on stimulation with IL-15, IL-18, and IL-12. In these settings, sorted splenic KLRG1$^-$ NK cells were characterized by profound defects in acquiring both IRF-8 and KLRG1 expression in the absence of STAT4 (Fig. 3*E*). Moreover, when adoptively transferred in CD45.1 mice, FACS-sorted KLRG1$^-$ NK cells from *Ncr1*$^{\Delta Stat4}$ showed an impaired ability to differentiate in KLRG1$^+$ cells during intestinal inflammation (Fig. 3*F*).

Altogether, we provide evidence for a nonredundant role of STAT4 in driving the acquisition of a terminally differentiated NK cell phenotype during intestinal inflammation.

***Stat4* Deletion in ILC1 Elicits Gene Modules Associated with STAT5 Signaling during Intestinal Inflammation.** Since *Stat4*-deficient ILC1 showed a higher number of up-regulated genes compared with NK cells and enhanced differentiation toward the cytotoxic phenotype (Fig. 2 *B*, *E*, and *G*), we speculated that STAT4 expression could repress alternative signaling pathways selectively in ILC1 during intestinal inflammation. By performing single sample (ss)GSEA on NK cell and ILC1 transcriptional states, we noticed that gene signatures associated with cytokines activating STAT5 signaling (red boxes), such as IL-2, IL-7, and IL-15, were significantly induced in *Stat4*-deficient ILC1$_d$ (Fig. 4 *A* and *B*). As control, we included gene signatures associated with the IL-12/STAT4 pathway, which were significantly decreased in these cells (blue boxes in Fig. 4 *A* and *B*). These results suggest that STAT4 could paradoxically counteract the functions of cytokines acting through STAT5 during intestinal inflammation, restraining effector differentiation of ILC1.

Since the absence of *Stat4* in lilp NCR$^+$ innate lymphocytes did not favor STAT5 phosphorylation upon short treatment with IL-12 in ILC1 (*SI Appendix*, Fig. S4*E*), we investigated whether the function of cytokines inducing STAT5 might be altered in ILC1 from *Ncr1*$^{\Delta Stat4}$ mice. Stimulation with IL-2, used as a prototypical STAT5 activator, resulted in similar pSTAT5 levels in ILC1 isolated from both *Stat4*$^{fl/fl}$ and *Ncr1*$^{\Delta Stat4}$ mice (Fig. 4*C*).

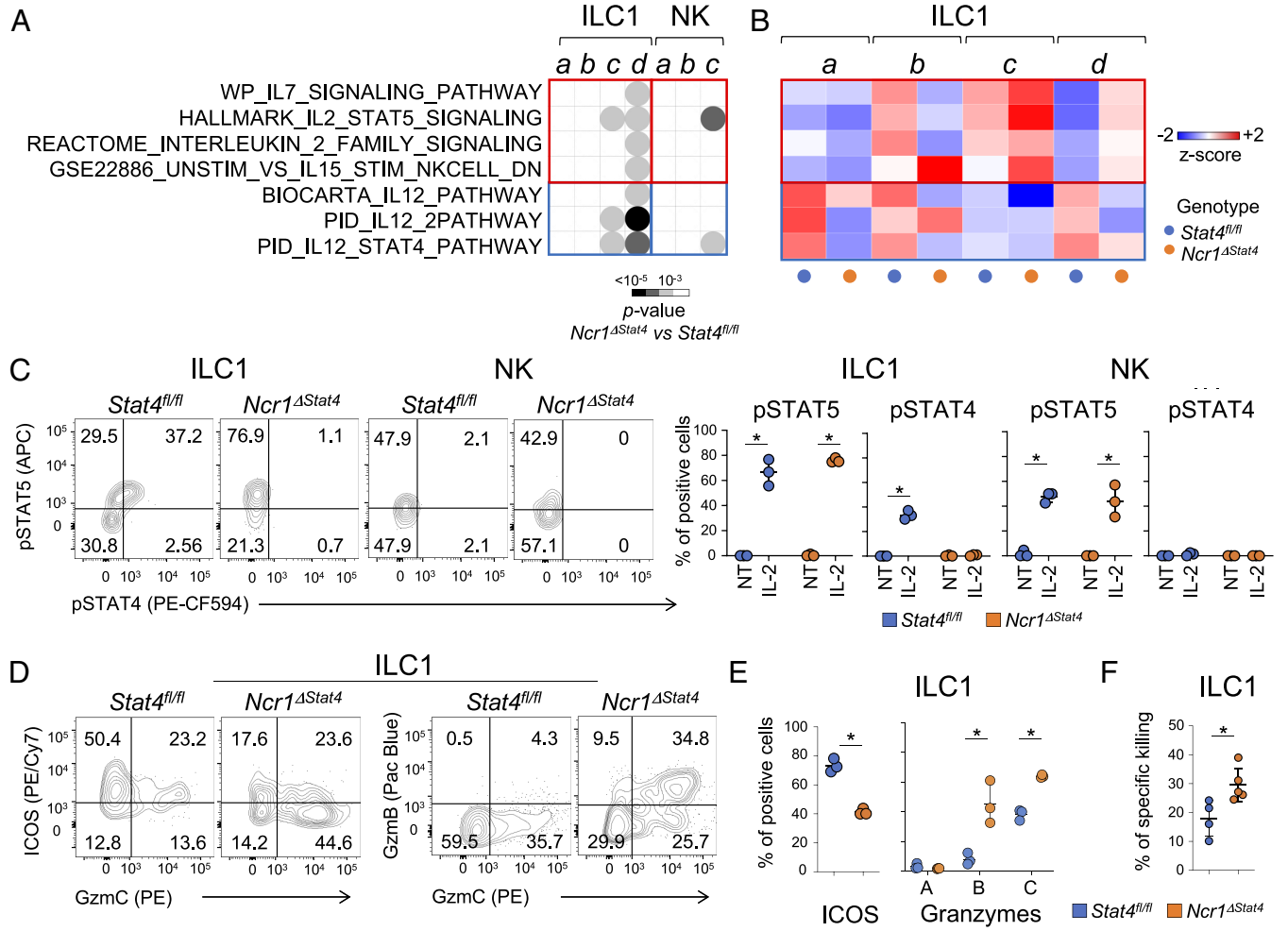

Fig. 4. Cytokines inducing STAT5 enhance generation of cytotoxic ILC1 in *Ncr1*$^{\Delta Stat4}$ mice. (*A*) The heat map shows the *P* values for the ssGSEA for gene sets associated with STAT5 and STAT4 signaling from the Molecular Signatures Database (MSigDB). ILC1 and NK cell clusters from *Stat4*$^{fl/fl}$ and *Ncr1*$^{\Delta Stat4}$ mice were compared. Gene sets with *P* value lower than 10^{-3} were visualized using a gray scale. (*B*) The heat map represents the z-score defined using the median expression of gene sets selected in panel *B* across ILC1 transcriptional states. (*C*) Flow cytometry contour plots and scatter plots show the expression of pSTAT5 and pSTAT4 in lilp ILC1 and NK cells from *Stat4*$^{fl/fl}$ and *Ncr1*$^{\Delta Stat4}$ mice, following ex vivo stimulation with IL-2 (1,000 IU/mL), for 30 min. A representative experiment out of two independent experiments performed is shown; (n = 3, per group). (*D*) Flow cytometry contour plots show the expression of GzmC, GzmB, and ICOS in ILC1 from *Stat4*$^{fl/fl}$ and *Ncr1*$^{\Delta Stat4}$ mice, upon ex vivo stimulation with IL-2 (1,000 IU/mL), for 24 h. (*E*) The scatter plots show the percentage of ICOS$^+$, GzmA$^+$, GzmB$^+$, and GzmC$^+$ ILC1 from *Stat4*$^{fl/fl}$ and *Ncr1*$^{\Delta Stat4}$ mice, upon ex vivo stimulation with IL-2 (1,000 IU/mL), for 24 h. Representative data of three independent experiments performed are shown; at least 6 mice per group were used. (*F*) The scatter plot displays the percentage of specific killing of IL-2 activated ILC1 from *Stat4*$^{fl/fl}$ and *Ncr1*$^{\Delta Stat4}$ mice against YAC-1 cells at an effector:target ratio of 25:1.

Strikingly, despite the known preference for STAT5 activation, IL-2 also induced phosphorylation of STAT4 in ILC1 (Fig. 4*C*). This property was shared with IL-15 (*SI Appendix*, Fig. S4*F*), suggesting that STAT4 could directly act downstream of cytokines signaling via IL-2Rγ, limiting the functions of innate lymphocytes during activation.

To corroborate this hypothesis, we employed an in vitro system to track whether *Stat4*-deficient ILC1 effector differentiation was altered upon IL-2 activation. Mimicking the enhanced effector differentiation observed in vivo during acute colitis, IL-2 stimulation led ILC1 from $Ncr1^{\Delta Stat4}$ mice to express lower levels of ICOS and higher levels of GzmC and GzmB than ILC1 from $Stat4^{fl/fl}$ mice (Fig. 4 *D* and *E*); GzmA instead was not induced (Fig. 4*E*). In line with the increased expression of granzymes, *Stat4*-deficient ILC1 were more cytotoxic against YAC-1 cells than *Stat4*-sufficient ILC1 (Fig. 4*F*). To evaluate whether this mechanism of regulation was conserved among ILC1 from distinct tissues, we stimulated ILC1 isolated from the small intestinal lamina propria (silp) and liver with IL-2. Similar to the findings obtained using lilp ILC1, IL-2 was able to trigger higher levels of GzmB and GzmC in silp and hepatic ILC1 from $Ncr1^{\Delta Stat4}$ mice (*SI Appendix*, Fig. S4*G*). In contrast with lilp ILC1, GzmA expression was also enhanced in *Stat4*-deficient silp and hepatic ILC1, highlighting the distinct mechanisms of effector differentiation existing among ILC1 from different tissues.

Altogether, by using ex vivo and in vitro systems, we show that STAT4 activation induced by cytokines using IL-2Rγ/STAT5 for signaling is able to limit the effector differentiation of ILC1.

STAT4 Deletion in NCR^+ Innate Lymphocytes Unleashes Pathogenic IL-13-Production from T cells during Acute Colitis Induced by DSS. Previous evidence has shown that mice carrying germline deletion of STAT4 are more susceptible to intestinal inflammation induced by DSS due to defects in both Th1 and Th17 responses (61). Since innate lymphocytes can control several aspects of intestinal $CD4^+$ T cell biology, including maintenance of Treg cells (62, 63), we hypothesized that deletion of *Stat4* in innate lymphocytes could alter $CD4^+$ T cell functions, contributing to promote intestinal inflammation. Despite the global reduction of the IFN-γ levels in $Ncr1^{\Delta Stat4}$ mice, we did not detect differences in the frequency of both IFN-γ- and IL-17-producing $CD4^+$ T cells (Fig. 5*A* and *SI Appendix*, Fig. S1*A* for gating strategy). Similarly, we did not observe significant changes in the percentage of Treg cells (Fig. 5*A*). In contrast, the frequency of IL-13- and IL-5-producing $CD4^+$ T cells was significantly increased in DSS-treated $Ncr1^{\Delta Stat4}$ mice (Fig. 5*B*).

In vivo blockade of IL-13 using a neutralizing antibody protected both $Stat4^{fl/fl}$ and $Ncr1^{\Delta Stat4}$ mice from developing severe colitis induced by 3% DSS administration, with mice treated with the anti-IL-13 antibody showing lower body weight loss and DAI compared with control groups (Fig. 5 *C* and *D*). On the other hand, we found no significant differences in DAI scores by the comparison of $Ncr1^{\Delta Stat4}$ and $Stat4^{fl/fl}$ mice treated with anti-IL-13 antibody.

Collectively, our data indicate that the increased levels of IL-13-producing $CD4^+$ T cells contribute to enhance intestinal inflammation in $Ncr1^{\Delta Stat4}$ mice.

Discussion

Here, by using a mouse model, we have unraveled different modalities of STAT4 regulation in ILC1 and NK cells, which give this TF a central role in restraining intestinal inflammation induced by DSS. By integrating transcriptomic and genetic approaches, we revealed that the inflamed large intestine contains ILC1 with distinct effector phenotypes. Paradoxically, *Stat4* deficiency in mice leads to a higher propensity to generate cytotoxic ILC1 during intestinal inflammation and to unleash signals associated to cytokines activating STAT5. In sharp contrast with the effects observed in ILC1, we delineated a nonredundant role for STAT4 in driving the acquisition of the NK cell effector phenotype. In the absence of *Stat4*, NK cells show defects in inducing genes associated with stretched- or super-enhancer structure, which overall affect the inflammation-driven formation of terminally differentiated cells. While STAT4 is widely expressed by both NK cells and ILC1, the higher impact of its deletion on the differentiated subsets might be due to cumulative effects occurring during the effector differentiation driven by intestinal inflammation.

NK cells have been employed as a model to study transcriptional and epigenetic regulation mediated by STATs in innate lymphocytes (33, 64). Cytokine-stimulated NK cells show widespread colocalization of STAT4 and STAT5 at enhancer sites, which is associated with the formation of active enhancers and high-magnitude gene induction (33). Moreover, simultaneous activation of STAT4 (through IL-12) and STAT5 (IL-2, IL-15) is known to produce additive and/or synergistic effects in adaptive and innate cells (65). Thus, our data showing that STAT4 activation induced by IL-2 can have inhibitory roles in ILC1 are unexpected. Several cytokines can activate multiple STATs in a cell type–dependent manner (50), including type I IFNs, which can mainly activate STAT4 and STAT1 in NK cells (29), or IL-2, which can activate JAK2 and STAT4 in resting human NK cells, but fails in inducing pSTAT4 in T cells (66). In this regard, our data provide evidence of how STAT4 can drive cell type–dependent outcomes during intestinal inflammation. Many factors can account for the differential behavior of *Stat4*-deficient ILC1 and NK cells, including the higher sensitivity of ILC1 toward IL-2, compared with NK cells. Since STAT5 phosphorylation is not altered in the absence of *Stat4* in ILC1, our model suggests that STAT4 and STAT5 can compete at the genomic level, limiting ILC1 effector differentiation during inflammation.

Our data also reveal that STAT4 expression in innate lymphocytes contributes to restrain intestinal inflammation in the DSS-induced colitis model. In line with our results, mice carrying germline deletion of the prototypical type 1 TFs, T-bet and STAT4, are more susceptible to intestinal inflammation induced by DSS, due to defects in T cell and myeloid cell responses, or alterations of the gut intestinal microbiota (61, 67). It is important to consider that T-bet and STAT4 play detrimental roles in the T cell transfer model (68, 69), where the expression of these TFs is required for generation of pathogenic Th17 able to produce both IL-17 and IFN-γ (65). As for T cells, STAT4 is critically required for the production of IFN-γ by NCR^+ innate lymphocytes; however, decreased levels of this cytokine do not lead to a lower degree of inflammation in $Ncr1^{\Delta Stat4}$ mice in the DSS model. Thus, our data are in agreement with clinical studies showing that antibody-mediated neutralization of IFN-γ by fontolizumab is not associated with strong clinical response (70–72). Moreover, recent findings show that constitutive activation of STAT5 in ILC1 leads to lethal autoimmunity in neonatal mice in a perforin-dependent manner (8). Thus, an increase of cytotoxic ILC1 has the potential to amplify gut inflammation in $Ncr1^{\Delta Stat4}$ mice.

We also observed that STAT4 expression in innate lymphocytes indirectly controls the number of Th2 in the inflamed intestine. Recently, by using models of mixed type 1-type 2 inflammation, it has been observed that the production of IFN-γ from adaptive and innate cells is able to suppress generation of IL-5- and

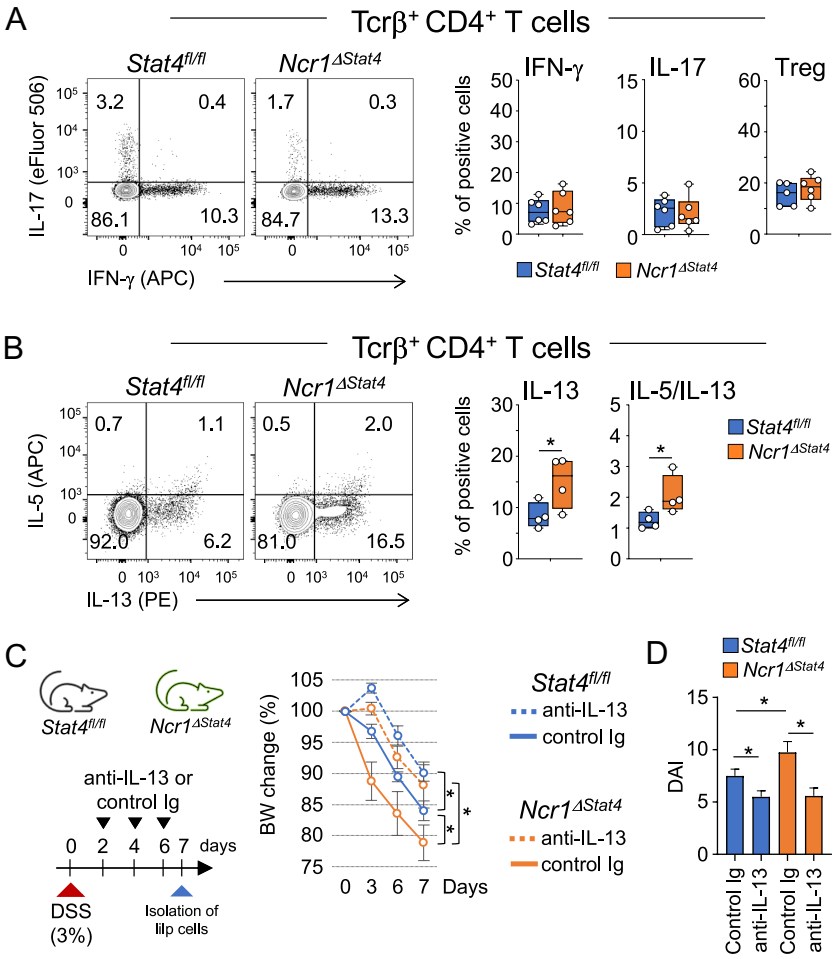

Fig. 5. Altered CD4$^+$ T cell response in *Ncr1*$^{\Delta Stat4}$ mice during intestinal inflammation. (*A*) Flow cytometry contour plots and box plots show the percentage of IFN-γ and IL-17 expressing cells and Treg cells within CD3ε$^+$NK1.1$^-$Tcrβ$^+$CD4$^+$CD8$^-$ T cells upon stimulation with PMA/Ionomycin in the lilp of DSS-treated *Stat4*$^{fl/fl}$ and *Ncr1*$^{\Delta stat4}$ mice. Tregs were defined as FoxP3$^+$ cells among the total CD3ε$^+$NK1.1$^-$Tcrβ$^+$CD4$^+$ T cells (*SI Appendix*, Fig. S1*A*). (*B*) Flow cytometry contour plots and box plots show the percentage of IL-5 and IL-13 expressing cells within CD3ε$^+$NK1.1$^-$Tcrβ$^+$CD4$^+$CD8$^-$ T cells upon stimulation with PMA/Ionomycin in the lilp of DSS-treated *Stat4*$^{fl/fl}$ and *Ncr1*$^{\Delta stat4}$ mice. (*A* and *B*) Representative data from at least three independent experiments performed are shown; n = 4 to 6 per group for each experiment. (*C* and *D*) Anti-IL-13 antibody and control Ig were administered to *Stat4*$^{fl/fl}$ and *Ncr1*$^{\Delta Stat4}$ mice at days 2, 4, and 6 of DSS treatment in three independent experiments. The line chart depicts the body weight change, expressed as a percentage of initial weight. Data provided represent the mean ± SEM of the percentage body weight from a representative experiment. The bar plot shows the DAI for *Stat4*$^{fl/fl}$ and *Ncr1*$^{\Delta Stat4}$ mice administered with control Ig (*C*) or anti-IL-13 antibody of pooled data from three independent experiments. For statistical analysis, multiple unpaired Student's *t* test (*A*, *B*, and *D*) and Wilcoxon signed-rank test (*C*) were used.

IL-13-producing ILC2 and Th2 cells, restraining lethality associated with *Listeria monocytogenes* infection (73). Since we show that targeting STAT4 expression in type 1 innate lymphocytes leads to increased production of IL-13 in CD4$^+$ T cells, a similar cross talk by type 1 innate lymphocytes and T cells might also apply to the model of DSS-colitis, where IL-13 function has been shown to be detrimental (74, 75) and contributes to increase the inflammation observed in *Ncr1*$^{\Delta Stat4}$ mice.

Aside from the recognized limitations, preclinical in vivo models represent fast and reproducible systems to study distinct aspects of human pathology (76). In this context, understanding mechanisms underlying STAT4 functions in innate lymphocytes is particularly relevant in the context of human IBD since this TF is downstream of IL-12 and IL-23 signaling (30) and the blockade of the common IL-12/23 subunit IL-12p40 is effective treatment for CD patients (77–79). Both mouse studies and clinical data suggest a major role for IL-23, over IL-12, in driving the intestinal inflammation (80–85). However, by targeting STAT4, which blocks most of the biological effects of IL-12, we revealed different aspects of regulation of intestinal inflammation mediated by type 1 innate lymphocytes, which resulted to be protective, rather than detrimental. Finally, our data further suggest that a broader strategy, based on inhibiting multiple JAKs and/or multiple cytokines in the context of IBD, may result in better clinical outcomes.

Materials and Methods

Mouse Models. C57BL/6J and CD45.1 (Jackson mouse stock no. 008449) mice were purchased from Charles River. *Ncr1*$^{greenCre/+}$ (54) and *Rorc*(γt) Cre × ROSA26-YFP (RORγt-FM reporter) (46) mice were generated previously. *Stat4fl/fl* mice were generated in this study through Ozgene Pty Ltd (Bentley WA, Australia). The targeting construct was electroporated into a C57BL/6 ES cell line, Bruce4 (86). Homologous recombinant ES cell clones were identified by qPCR and injected into goGermline™ blastocysts (87). Male chimeric mice were obtained and crossed to a ubiquitous FLP C57BL/6J mouse line to remove the FRT-flanked selectable marker cassette and to establish heterozygous germline offspring on C57BL/6 background. The heterozygous mice were then intercrossed to generate a homozygous mouse line. *Ncr1*$^{greenCre/+}$ mice were then crossed with *Stat4*$^{fl/fl}$ mice. All the experiments were performed using littermates. Mice were housed in individually ventilated cages under specific pathogen-free conditions. All the experiments were performed using 6 to 10 wk old mice. All animal studies have been approved by the Italian Ministry of Health and performed in conformity with the directive 2010/63/UE. For sample size, see corresponding figure legends.

DSS Colitis. Mice received 2 or 3% DSS (Mw ~40,000, 42867, Sigma-Aldrich) in sterile drinking water ad libitum for 7 d, as indicated in figure legends. After weaning, *Ncr1*$^{\Delta Stat4}$ and littermates *Stat4*$^{fl/fl}$ mice were cohoused until the beginning of the DSS treatment to minimize the influence of the microbiota. For in vivo antibody administration, mice were injected intraperitoneally with neutralizing mAb against IL-13 (clone 8H8, InvivoGen), 100 μg at days 2, 4, and 6 of DSS treatment. The DAI was calculated as previously established (88). The following parameters were used at day 7 and evaluated by a blinded operator: weight loss, stool consistency, fecal blood, and rectal bleeding. For weight loss: 0 = no loss, 1 = 1 to 5%, 2 = 5 to 10%, 3 = 10 to 20%, and 4 = >20%. For stool consistency: 0 = normal, 1 = soft, 2 = very soft, and 3 = diarrhea. For fecal blood: 0 = no blood, 1 = red, 2 = dark red, and 3 = black. For rectal bleeding: 0 = no blood, 1 = red, 2 = dark red, and 3 = gross bleeding.

Cell Isolation. Cells from the large and small intestinal lamina propria were isolated after incubation of the intestine in RPMI with 0.5 mg/mL DNase I and 0.25 mg/mL Liberase TL (Roche) and purification with 40% Percoll (Cytiva), as indicated in ref. 89. Cells from the spleen were obtained after mechanical dissociation and filtration through 70 μm cell strainer filters. Cells from the liver were obtained after mechanical dissociation and filtration through 70 μm cell strainer filters. Next, lymphocytes were isolated by density gradient centrifugation using Lympholyte cell separation media. Cells from bone marrow were isolated by extensive flushing of femurs and tibias with PBS.

Ex Vivo Assays. Cells were cultured in Roswell Park Memorial Institute (RPMI) medium with 10% (vol/vol) FCS, 2 mM glutamine, 100 IU/mL of penicillin, 0.1 mg/mL of streptomycin, 20 mM N-(2-Hydroxyethyl)piperazine-N′-(2-ethanesulfonic acid) (HEPES) buffer, pH 7.2 to 7.5, 1 mM sodium pyruvate, nonessential amino acids (all from Thermo Fisher Scientific), and 2 μM β-mercaptoethanol (Sigma-Aldrich). Cytokines were used at the following concentrations: IL-2 (1,000 IU/mL, R&D systems), IL-12 (10 to 100 ng/mL, PeproTech), IL-15 (100 ng/mL, R&D systems), and IL-18 (10 to 100 ng/mL, R&D systems), according to the experiment design. T cells were stimulated using the phorbol 12-myristate 13-acetate (PMA)/Ionomycin-based cell stimulation cocktail (eBioscience). Golgi stop (Becton Dickinson) or Brefeldin A (Sigma Aldrich) was added for the evaluation of cytokine expression. The flow cytometry–based killing assay was performed as previously described (6). Briefly, lilp ILC1 were sorted and incubated with CFSE-labeled target cells (YAC-1) at 25:1 effector/target ratio for 4 h. CFSE-labeled cells alone were used as control. Cells were washed, and 20.000 APC-labeled microbeads (Spherotech) were added to each sample to allow the calculation of specific lysis.

Flow Cytometry and Fluorescence-activated Cell Sorting (FACS). Flow cytometry analysis was performed on a FACSCanto II or LSR Fortessa (Becton Dickinson). Cell sorting was performed using FACSAria III (Becton Dickinson); FACS-sorted cells were confirmed to be higher than 95% pure with postsort analysis. Dead cells were excluded by using Fixable Viability Stain 780 (Becton Dickinson), Zombie NIR™ Fixable Viability Kit (BioLegend), or Zombie Green™ Fixable Viability Kit (BioLegend). Antibodies used in this study can be found in *SI Appendix*. Flow cytometry data were analyzed using FlowJo_v10.8.1 (Beckton Dickinson).

Adoptive Transfer Experiments. For adoptive transfer experiments, cells were isolated from the spleen of *Stat4*$^{+/+}$, *Stat4*$^{fl/fl}$ or *Ncr1*$^{\Delta Stat4}$ mice and NK cells enriched by magnetic separation, using the NK Cell Isolation Kit, mouse (Miltenyi Biotec). Then, total NK cells were FACS-sorted as L/D$^-$CD3ε$^-$CD19$^-$NKp46$^+$ cells (*SI Appendix*, Fig. S3*I*), while KLRG1$^-$ NK cells were FACS-sorted as L/D$^-$CD3ε$^-$CD19$^-$NKp46$^+$KLRG1$^-$ cells (Fig. 3*G*). A total of 5 × 10^5 cells were intravenously injected (250 μL/injection) into syngeneic CD45.1 age-matched mice, which were administered with 2% DSS. After 7 d, recipient mice were killed for further analysis.

Enzyme-linked Immunosorbent Assay (ELISA). Serum was prepared after centrifugation of whole blood harvested from the tail vein. IFN-γ concentration was measured by using IFN gamma "Femto-HS" High Sensitivity Mouse Uncoated ELISA Kit with Plates (Thermo Fisher).

Statistical Analysis. Detailed information concerning the number of mice analyzed and the statistical methods used is provided in the figure legends. "n" represents the number of mice analyzed in each experiment. Experiments were repeated at least two times as a control for experimental variation. For statistical analysis of comparison between groups, unpaired Student's *t* test was used. One-way or two-way ANOVA was used to analyze experiments with multiple groups and two independent variables. All statistical analyses were performed using the Prism software version 8.0.2 (GraphPad). Data with *P* values less than 0.05 were considered significantly different and indicated with stars.

Data, Materials, and Software Availability. All data are included in the manuscript and/or supporting information. The scRNA-seq and bulkRNA-seq data have been deposited in the GEO under accession numbers GSE210977 and GSE210483 (90).

ACKNOWLEDGMENTS. We are grateful to Manuel O. Jakob for technical assistance. This work was supported by the Italian Association for Cancer Research (AIRC) (MFAG-21311 G. Sciumè; 5×1000-21147 A.S.; IG-20766 S.S.; AIRC fellowship for Italy 2020-25307 M.L.); The Institut Pasteur (France) (Transversal Research Program (PTR-113-17 G. Sciumè, J.P.D.S., C.A.J.V., and A.S.; PTR-550-22; G. Sciumè, C.A.J.V.); Istituto Pasteur Italia-Fondazione Cenci Bolognetti (Under 45-213 G. Sciumè); The Japan Society for the Promotion of Science (JSPS) (Grant-in-Aid for Transformative Research Areas(B): 21H05123 Y.M.); PRIN (20174T7NXL_003 A.G.); Marie Skłodowska-Curie Actions (MSCA) Innovative Training Networks (ITN): H2020-MSCA ITN-2019 (grant agreement No 813343 J.M.); and DFG Priority Program 1937 (DI 764/7-2, DI 764/9-2 A.D.)

Author affiliations: [a]Department of Molecular Medicine, Sapienza University of Rome, Rome 00161, Italy; [b]Laboratory affiliated to Istituto Pasteur Italia–Fondazione Cenci Bolognetti, Rome 00161, Italy; [c]Laboratory of Innate Immunity, Institute of Microbiology, Infectious Diseases and Immunology, Charité–Universitätsmedizin Berlin, Corporate Member of Freie Universität Berlin and Humboldt–Universität zu Berlin, Campus Benjamin Franklin, Berlin 12203, Germany; [d]Mucosal and Developmental Immunology, Deutsches Rheuma-Forschungszentrum, an Institute of the Leibniz Association, Berlin 10117, Germany; [e]Center for Life Nano- & Neuro-Science, Istituto Italiano di Tecnologia, Rome 00161, Italy; [f]Biodata Mining and Discovery Section, Office of Science and Technology, National Institute of Arthritis, Musculoskeletal and Skin Diseases, NIH, Bethesda, MD 20892; [g]Translational Immunology Section, Office of Science and Technology, National Institute of Arthritis, Musculoskeletal and Skin Diseases, NIH, Bethesda, MD 20892; [h]Division of Gastroenterology and Hepatology, Department of Internal Medicine, Keio University School of Medicine, Tokyo 1608582, Japan; [i]Istituti di Ricovero e Cura a Carattere Scientifico Neuromed, Isernia 86077, Italy; and [j]Innate Immunity Unit, Institut Pasteur, Université Paris Cité, INSERM U1223, Paris 75724, France

1. A. N. J. McKenzie, H. Spits, G. Eberl, Innate lymphoid cells in inflammation and immunity. *Immunity* **41**, 366–374 (2014).
2. N. Branzk, K. Gronke, A. Diefenbach, Innate lymphoid cells, mediators of tissue homeostasis, adaptation and disease tolerance. *Immunol. Rev.* **286**, 86–101 (2018).
3. E. Vivier *et al.*, Innate lymphoid cells: 10 years on. *Cell* **174**, 1054–1066 (2018).
4. L. Riggan, A. G. Freud, T. E. O'Sullivan, True detective: Unraveling group 1 innate lymphocyte heterogeneity. *Trends Immunol.* **40**, 909–921 (2019).
5. V. S. Cortez, M. Colonna, Diversity and function of group 1 innate lymphoid cells. *Immunol. Lett.* **179**, 19–24 (2016).
6. C. Di Censo *et al.*, Granzyme A and CD160 expression delineates ILC1 with graded functions in the mouse liver. *Eur. J. Immunol.* **51**, 2568–2575 (2021).
7. C. Friedrich *et al.*, Effector differentiation downstream of lineage commitment in ILC1s is driven by Hobit across tissues. *Nat. Immunol.* **22**, 1256–1267 (2021).
8. B. G. Nixon *et al.*, Cytotoxic granzyme C-expressing ILC1s contribute to antitumor immunity and neonatal autoimmunity. *Sci. Immunol.* **7**, eabi8642 (2022).
9. Y. Gao *et al.*, Tumor immunoevasion by the conversion of effector NK cells into type 1 innate lymphoid cells. *Nat. Immunol.* **18**, 1004–1015 (2017).
10. E. Park *et al.*, Toxoplasma gondii infection drives conversion of NK cells into ILC1-like cells. *Elife* **8**, e47605 (2019).
11. C. Seillet, L. Brossay, E. Vivier, Natural killers or ILC1s? That is the question *Curr. Opin. Immunol.* **68**, 48–53 (2021).
12. H.-Y. Shih *et al.*, Developmental acquisition of regulomes underlies innate lymphoid cell functionality. *Cell* **165**, 1120–1133 (2016).
13. O. I. Koues *et al.*, Distinct gene regulatory pathways for human innate versus adaptive lymphoid cells. *Cell* **165**, 1134–1146 (2016).
14. L. Chiossone *et al.*, Maturation of mouse NK cells is a 4-stage developmental program. *Blood* **113**, 5488–5496 (2009).
15. J. Zhang *et al.*, T-bet and Eomes govern differentiation and function of mouse and human NK cells and ILC1. *Eur. J. Immunol.* **48**, 738–750 (2018), 10.1002/eji.201747299.
16. D. Gotthardt, V. Sexl, STATs in NK-cells: The good, the bad, and the ugly. *Front. Immunol.* **7**, 694 (2016).
17. H. Stabile *et al.*, JAK/STAT signaling in regulation of innate lymphoid cells: The gods before the guardians. *Immunol. Rev.* **286**, 148–159 (2018).
18. S. M. Gordon *et al.*, The transcription factors T-bet and Eomes control key checkpoints of natural killer cell maturation. *Immunity* **36**, 55–67 (2012).

19. G. Sciumé *et al.*, Distinct requirements for T-bet in gut innate lymphoid cells. *J. Exp. Med.* **209**, 2331–2338 (2012).
20. C. S. N. Klose *et al.*, Differentiation of type 1 ILCs from a common progenitor to all helper-like innate lymphoid cell lineages. *Cell* **157**, 340–356 (2014).
21. M. J. Townsend *et al.*, T-bet regulates the terminal maturation and homeostasis of NK and Valpha14i NKT cells. *Immunity* **20**, 477–494 (2004).
22. C. Daussy *et al.*, T-bet and Eomes instruct the development of two distinct natural killer cell lineages in the liver and in the bone marrow. *J. Exp. Med.* **211**, 563–577 (2014).
23. J. Zhang *et al.*, Sequential actions of EOMES and T-BET promote stepwise maturation of natural killer cells. *Nat. Commun.* **12**, 5446 (2021).
24. R. Yang *et al.*, Human T-bet governs innate and innate-like adaptive IFN-γ immunity against mycobacteria. *Cell* **183**, 1826–1847.e31 (2020).
25. W. E. Thierfelder *et al.*, Requirement for Stat4 in interleukin-12-mediated responses of natural killer and T cells. *Nature* **382**, 171–174 (1996).
26. M. H. Kaplan, Y. L. Sun, T. Hoey, M. J. Grusby, Impaired IL-12 responses and enhanced development of Th2 cells in Stat4-deficient mice. *Nature* **382**, 174–177 (1996).
27. C. S. N. Klose *et al.*, A T-bet gradient controls the fate and function of CCR6-RORγt+ innate lymphoid cells. *Nature* **494**, 261–265 (2013).
28. Y. Mikami *et al.*, NCR+ ILC3 maintain larger STAT4 reservoir via T-BET to regulate type 1 features upon IL-23 stimulation in mice. *Eur. J. Immunol.* **48**, 1174–1180 (2018), 10.1002/eji.201847480.
29. T. Miyagi *et al.*, High basal STAT4 balanced by STAT1 induction to control type 1 interferon effects in natural killer cells. *J. Exp. Med.* **204**, 2383–2396 (2007).
30. W. T. Watford *et al.*, Signaling by IL-12 and IL-23 and the immunoregulatory roles of STAT4. *Immunol. Rev.* **202**, 139–156 (2004).
31. J. C. Sun *et al.*, Proinflammatory cytokine signaling required for the generation of natural killer cell memory. *J. Exp. Med.* **209**, 947–954 (2012).
32. O.-E. Weizman *et al.*, ILC1 confer early host protection at initial sites of viral infection. *Cell* **171**, 795–808.e12 (2017).
33. G. Sciumè *et al.*, Rapid enhancer remodeling and transcription factor repurposing enable high magnitude gene induction upon acute activation of NK cells. *Immunity* **53**, 745–758.e4 (2020).
34. C. M. Lau *et al.*, Epigenetic control of innate and adaptive immune memory. *Nat. Immunol.* **19**, 963–972 (2018).
35. H. Morita, K. Moro, S. Koyasu, Innate lymphoid cells in allergic and nonallergic inflammation. *J. Allergy Clin. Immunol.* **138**, 1253–1264 (2016).
36. A. Geremia, C. V. Arancibia-Cárcamo, Innate lymphoid cells in intestinal inflammation. *Front. Immunol.* **8**, 1296 (2017).
37. C. Pearson, H. H. Uhlig, F. Powrie, Lymphoid microenvironments and innate lymphoid cells in the gut. *Trends Immunol.* **33**, 289–296 (2012).
38. G. F. Sonnenberg, D. Artis, Innate lymphoid cells in the initiation, regulation and resolution of inflammation. *Nat. Med.* **21**, 698–708 (2015).
39. D. R. Withers, M. R. Hepworth, Group 3 innate lymphoid cells: Communications hubs of the intestinal immune system. *Front. Immunol.* **8**, 1298 (2017).
40. L. Mazzurana *et al.*, Crohn's disease is associated with activation of circulating innate lymphoid cells. *Inflamm. Bowel. Dis.* **27**, 1128–1138 (2021).
41. M. Forkel *et al.*, Distinct alterations in the composition of mucosal innate lymphoid cells in newly diagnosed and established crohn's disease and ulcerative colitis. *J. Crohns. Colitis.* **13**, 67–78 (2019).
42. M. Friedrich, M. Pohin, F. Powrie, Cytokine networks in the pathophysiology of inflammatory bowel disease. *Immunity* **50**, 992–1006 (2019).
43. J. H. Bernink *et al.*, Human type 1 innate lymphoid cells accumulate in inflamed mucosal tissues. *Nat. Immunol.* **14**, 221–229 (2013).
44. M. Forkel, J. Mjösberg, Dysregulation of group 3 innate lymphoid cells in the pathogenesis of inflammatory bowel disease. *Curr. Allergy Asthma Rep.* **16**, 73 (2016).
45. J. H. Bernink *et al.*, Interleukin-12 and -23 control plasticity of CD127(+) group 1 and group 3 innate lymphoid cells in the intestinal lamina propria. *Immunity* **43**, 146–160 (2015).
46. C. Vonarbourg *et al.*, Regulated expression of nuclear receptor RORγt confers distinct functional fates to NK cell receptor-expressing RORγt(+) innate lymphocytes. *Immunity* **33**, 736–751 (2010).
47. S. Buonocore *et al.*, Innate lymphoid cells drive interleukin-23-dependent innate intestinal pathology. *Nature* **464**, 1371–1375 (2010).
48. L. J. Hall *et al.*, Natural killer cells protect mice from DSS-induced colitis by regulating neutrophil function via the NKG2A receptor. *Mucosal. Immunol.* **6**, 1016–1026 (2013).
49. U. Bank *et al.*, c-FLIP is crucial for IL-7/IL-15-dependent NKp46+ ILC development and protection from intestinal inflammation in mice. *Nat. Commun.* **11**, 1056 (2020).
50. A. V. Villarino, Y. Kanno, J. J. O'Shea, Mechanisms and consequences of Jak-STAT signaling in the immune system. *Nat. Immunol.* **18**, 374–384 (2017).
51. A. Franke *et al.*, Genome-wide meta-analysis increases to 71 the number of confirmed Crohn's disease susceptibility loci. *Nat. Genet.* **42**, 1118–1125 (2010).
52. D. P. B. McGovern *et al.*, Genome-wide association identifies multiple ulcerative colitis susceptibility loci. *Nat. Genet.* **42**, 332–337 (2010).
53. A. Salas *et al.*, JAK-STAT pathway targeting for the treatment of inflammatory bowel disease. *Nat. Rev. Gastroenterol. Hepatol.* **17**, 323–337 (2020).
54. L. Ben Merzoug *et al.*, Conditional ablation of NKp46+ cells using a novel Ncr1(greenCre) mouse strain: NK cells are essential for protection against pulmonary B16 metastases. *Eur. J. Immunol.* **44**, 3380–3391 (2014).
55. S. J. Dulson, E. E. Watkins, D. K. Crossman, L. E. Harrington, STAT4 directs a protective innate lymphoid cell response to gastrointestinal infection. *J. Immunol.* **203**, 2472–2484 (2019).
56. L. C. Rankin *et al.*, Complementarity and redundancy of IL-22-producing innate lymphoid cells. *Nat. Immunol.* **17**, 179–186 (2016).
57. C. Song *et al.*, Unique and redundant functions of NKp46+ ILC3s in models of intestinal inflammation. *J. Exp. Med.* **212**, 1869–1882 (2015).
58. K. Yomogida *et al.*, Hobit confers tissue-dependent programs to type 1 innate lymphoid cells. *Proc. Natl. Acad. Sci. U.S.A.* **118**, e2117965118 (2021).
59. A. Crinier *et al.*, High-dimensional single-cell analysis identifies organ-specific signatures and conserved NK cell subsets in humans and mice. *Immunity* **49**, 971–986.e5 (2018).
60. Y. Hikichi, Y. Motomura, O. Takeuchi, K. Moro, Posttranscriptional regulation of ILC2 homeostatic function via tristetraprolin. *J. Exp. Med.* **218**, e20210181 (2021).
61. Y. S. Zhang *et al.*, STAT4 activation by leukemia inhibitory factor confers a therapeutic effect on intestinal inflammation. *EMBO J.* **38**, e99595 (2019).
62. L. Zhou *et al.*, Innate lymphoid cells support regulatory T cells in the intestine through interleukin-2. *Nature* **568**, 405–409 (2019).
63. M. R. Hepworth, G. F. Sonnenberg, Regulation of the adaptive immune system by innate lymphoid cells. *Curr. Opin. Immunol.* **27**, 75–82 (2014).
64. G. M. Wiedemann *et al.*, Deconvoluting global cytokine signaling networks in natural killer cells. *Nat. Immunol.* **22**, 627–638 (2021).
65. M. Kobayashi *et al.*, Identification and purification of natural killer cell stimulatory factor (NKSF), a cytokine with multiple biologic effects on human lymphocytes. *J. Exp. Med.* **170**, 827–845 (1989).
66. K. S. Wang, J. Ritz, D. A. Frank, IL-2 induces STAT4 activation in primary NK cells and NK cell lines, but not in T cells. *J. Immunol.* **162**, 299–304 (1999).
67. W. S. Garrett *et al.*, Communicable ulcerative colitis induced by T-bet deficiency in the innate immune system. *Cell* **131**, 33–45 (2007).
68. M. F. Neurath *et al.*, The transcription factor T-bet regulates mucosal T cell activation in experimental colitis and Crohn's disease. *J. Exp. Med.* **195**, 1129–1143 (2002).
69. S. J. Simpson *et al.*, T cell-mediated pathology in two models of experimental colitis depends predominantly on the interleukin 12/Signal transducer and activator of transcription (Stat)-4 pathway, but is not conditional on interferon gamma expression by T cells. *J. Exp. Med.* **187**, 1225–1234 (1998).
70. D. W. Hommes, S. J. van Deventer, Anti- and proinflammatory cytokines in the pathogenesis of tissue damage in Crohn's disease. *Curr. Opin. Clin. Nutr. Metab. Care* **3**, 191–195 (2000).
71. W. Reinisch *et al.*, Fontolizumab in moderate to severe Crohn's disease: A phase 2, randomized, double-blind, placebo-controlled, multiple-dose study. *Inflamm. Bowel. Dis.* **16**, 233–242 (2010).
72. W. Reinisch *et al.*, A dose escalating, placebo controlled, double blind, single dose and multidose, safety and tolerability study of fontolizumab, a humanised anti-interferon gamma antibody, in patients with moderate to severe Crohn's disease. *Gut* **55**, 1138–1144 (2006).
73. K. M. Cautivo *et al.*, Interferon gamma constrains type 2 lymphocyte niche boundaries during mixed inflammation. *Immunity* **55**, 254–271.e7 (2022).
74. M. S. Shajib *et al.*, Interleukin 13 and serotonin: Linking the immune and endocrine systems in murine models of intestinal inflammation. *PLoS One* **8**, e72774 (2013).
75. A. Hertati, S. Hayashi, Y. Ogawa, T. Yamamoto, M. Kadowaki, Interleukin-4 receptor α subunit deficiency alleviates murine intestinal inflammation in vivo through the enhancement of intestinal mucosal barrier function. *Front. Pharmacol.* **11**, 573470 (2020).
76. P. Kiesler, I. J. Fuss, W. Strober, Experimental models of inflammatory bowel diseases. *Cell Mol. Gastroenterol. Hepatol.* **1**, 154–170 (2015).
77. M. F. Neurath, Current and emerging therapeutic targets for IBD. *Nat. Rev. Gastroenterol. Hepatol.* **14**, 269–278 (2017).
78. B. G. Feagan *et al.*, Ustekinumab as induction and maintenance therapy for Crohn's disease. *N. Engl. J. Med.* **375**, 1946–1960 (2016).
79. B. E. Sands *et al.*, Ustekinumab as induction and maintenance therapy for ulcerative colitis. *N. Engl. J. Med.* **381**, 1201–1214 (2019).
80. I. C. Arnold *et al.*, CD11c(+) monocyte/macrophages promote chronic Helicobacter hepaticus-induced intestinal inflammation through the production of IL-23. *Mucosal. Immunol.* **9**, 352–363 (2016).
81. K. R. R. Siddiqui, S. Laffont, F. Powrie, E-cadherin marks a subset of inflammatory dendritic cells that promote T cell-mediated colitis. *Immunity* **32**, 557–567 (2010).
82. S. Hue *et al.*, Interleukin-23 drives innate and T cell-mediated intestinal inflammation. *J. Exp. Med.* **203**, 2473–2483 (2006).
83. H. H. Uhlig *et al.*, Differential activity of IL-12 and IL-23 in mucosal and systemic innate immune pathology. *Immunity* **25**, 309–318 (2006).
84. D. Yen *et al.*, IL-23 is essential for T cell-mediated colitis and promotes inflammation via IL-17 and IL-6. *J. Clin. Invest.* **116**, 1310–1316 (2006).
85. M. W. L. Teng *et al.*, IL-12 and IL-23 cytokines: From discovery to targeted therapies for immune-mediated inflammatory diseases. *Nat. Med.* **21**, 719–729 (2015).
86. F. Koentgen, G. Suess, D. Naf, Engineering the mouse genome to model human disease for drug discovery. *Methods Mol. Biol.* **602**, 55–77 (2010).
87. F. Koentgen *et al.*, Exclusive transmission of the embryonic stem cell-derived genome through the mouse germline. *Genesis* **54**, 326–333 (2016).
88. J. J. Kim, M. S. Shajib, M. M. Manocha, W. I. Khan, Investigating intestinal inflammation in DSS-induced model of IBD. *J. Vis. Exp.* 10.3791/3678 (2012).
89. G. Scarno, G. Pietropaolo, C. di Censo, G. Peruzzi, G. Sciumè, Assessing phosphorylation of STAT transcription factors in mouse innate lymphoid cells. *Methods Mol. Biol.* **2121**, 59–70 (2020).
90. G. Scarno *et al.*, Data for "Divergent roles for STAT4 in shaping differentiation of cytotoxic ILC1 and NK cells during gut inflammation." *Gene Expression Omnibus*. https://www.ncbi.nlm.nih.gov/geo/query/acc.cgi?acc=GSE211129. Deposited 12 August 2022.